Asian Research Journal of Current Science

Volume 6, Issue 1, Page 191-218, 2024; Article no.ARJOCS.1657

Statistical Study and Analysis of the Parameters in Forbush Effects and Interplanetary Disturbances (FEID) During Solar Cycles 23 and 24

O. P. Jerry-Okafor [a], C. C. Onuchukwu [a*], V. C. Okoye [a] and L. N. Okoli [b]

[a] Department of Industrial Physics, Chukwuemeka Odumegwu Ojukwu University, Uli Campus, Anambra State, Nigeria.
[b] Department of Computer Science Education, Madonna University Nigeria, Okija Cmapus, Anambra State, Nigeria.

Authors' contributions

This work was carried out in collaboration among all authors. All authors read and approved the final manuscript.

Article Information

Open Peer Review History:
This journal follows the Advanced Open Peer Review policy. Identity of the Reviewers, Editor(s) and additional Reviewers, peer review comments, different versions of the manuscript, comments of the editors, etc are available here: https://prh.globalpresshub.com/review-history/1657

Original Research Article

Received: 10/07/2024
Accepted: 14/09/2024
Published: 18/09/2024

ABSTRACT

A comprehensive statistical analysis of Forbush Effects and Interplanetary Disturbances (FEIDs) parameters during Solar Cycles (SCs) 23 and 24, spanning from 1996 to 2019 was performed. The Forbush Effect (FE) is characterized by a temporary reduction in cosmic ray (CR) flux observed on Earth, typically following solar CMEs, high-speed solar wind streams, and other solar eruptions. These reductions, known as Forbush Decreases (FDs), result from interactions between the solar wind, interplanetary magnetic fields, and galactic CR within Earth's magnetosphere. Interplanetary

---

**Corresponding author: Email: onuchukwu71chika@gmail.com;*

Cite as: *Jerry-Okafor, O. P., C. C. Onuchukwu, V. C. Okoye, and L. N. Okoli. 2024. "Statistical Study and Analysis of the Parameters in Forbush Effects and Interplanetary Disturbances (FEID) During Solar Cycles 23 and 24". Asian Research Journal of Current Science 6 (1):191-218. https://jofscience.com/index.php/ARJOCS/article/view/117.*

disturbances encompass a range of phenomena resulting from the interaction between solar wind and the Earth's magnetosphere, affecting space weather conditions significantly. The goal is to elucidate the temporal variations, interrelationships, and trends of key FEID parameters, thereby enhancing our understanding of solar-terrestrial interactions and space weather dynamics. The research utilizes data from the FEID database maintained by IZMIRAN, along with sunspot numbers (SSNs) from the Royal Observatory of Belgium. Key parameters analyzed include B_{max} (maximum interplanetary magnetic field intensity), V_mB_m (product of solar wind velocity and interplanetary magnetic field intensity), Bz_{min} (minimum value of the southward component of the interplanetary magnetic field (IMF)), Bz_mtoB_m (ratio of Bz minimum to B the maximum value of the interplanetary magnetic field), and ABz_{max} (maximum absolute value of the Bz component of the IMF) to explain the variations, interrelationships, and trends in these parameters and their impact on space weather and cosmic ray intensity (CRI) variations. Comprehensive statistical techniques, including time series analysis, correlation analysis, and trend analysis, were employed to examine the nearly two-and-a-half decades of data. The analysis reveals significant temporal variations and correlations among FEID parameters across SCs 23 and 24. During SC 23, a strong negative correlation was observed between B_{max} and SSNs, while SC 24 exhibited a weaker positive correlation. Similarly, Bz_{min} showed a strong inverse relationship with SSNs in SC 23, contrasting with a weaker positive correlation in SC 24. Time series analysis indicated that SC 24 generally exhibited higher B_{max} values and more pronounced fluctuations in V_mB_m compared to SC 23. Distribution plots revealed that parameters like Bz_{min} and ABz_{max} exhibited heavy-tailed distributions, indicating significant outliers and extreme values. The study underscores the importance of continuous monitoring and detailed statistical analysis to improve space weather forecasting and mitigate the impacts of solar disturbances on technological systems and human activities in space and on Earth.

Keywords: Forbush decrease; interplanetary disturbance; data analysis; geomagnetic index data analysis; geomagnetic index; solar wind; cosmic ray.

1. INTRODUCTION

The Sun, as the Earth's primary energy source, significantly influences space weather and terrestrial climate through its dynamic activities. These activities are manifested in various forms, including solar flares, coronal mass ejections (CMEs), and solar wind streams [1,2]. These solar activities directly or otherwise impact the variations of different parameters that determine the conditions of the space weather, which can impact the Earth's magnetosphere and ionosphere [3-7]. Studying these solar activities, particularly FEIDs, is crucial for understanding their impact on cosmic ray intensity (CRI) variations and space weather dynamics due to their impact on technology and geomagnetic disturbances [8].

The Forbush Effect (FE) is characterized by a temporary reduction in cosmic ray (CR) flux observed on Earth, typically following solar CMEs, high-speed solar wind streams, and other solar eruptions [9-12]. These reductions, known as Forbush Decreases (FDs), result from interactions between the solar wind, interplanetary magnetic fields, and galactic CR within Earth's magnetosphere. Interplanetary disturbances encompass a range of phenomena resulting from the interaction between solar wind and the Earth's magnetosphere, affecting space weather conditions significantly. FDs, first observed by Scott Forbush in 1937, are characterized by a sudden decrease in CRI followed by a gradual recovery [13,14]. These effects are typically associated with solar ejecta, such as CMEs and high-speed solar wind streams, which disturb the IMF and modulate CR flux [11,12,15]. Key characteristics of Forbush Effects include sudden onset; a rapid decrease in CR intensity, often within a few hours, and gradual recovery [16]. The CRI gradually returns to its original level over several days or weeks. The magnitude of the intensity of the decrease can vary, typically ranging from a few percent to as much as 20% [17,18].

FDs are categorized based on their origin and characteristics. The two primary types are Sporadic Forbush Decreases (SFDs) and Recurrent Forbush Decreases (RFDs) [19,20]. SFDs are associated with transient interplanetary events such as CMEs and solar flares and these events are characterized by: sudden onset, asymmetric profile, and transient nature [11,12,21-23]. RFDs are linked to high-speed solar wind streams emanating from coronal holes. These decreases exhibit gradual onset, symmetric profile, and periodic occurrence [24-27]. Understanding these types is crucial for interpreting CR intensity variations and their relationship with solar and interplanetary phenomena. These two kinds of FDs are detected using ground-based neutron monitors and muon detectors. These instruments measure the flux of CRs reaching the Earth's surface, providing data that reveals the extent and duration of the decreases. Observations from these detectors show that FDs can reduce CR intensity by up to 25%, with more intense events linked to stronger solar disturbances [12,28-30].

Interplanetary Disturbances refer to disruptions or fluctuations in the space environment between planets, caused by solar activities. These disturbances significantly influence space weather and can have various effects on Earth and its near-space environment [31-33, 66]. Major causes of interplanetary disturbances include CMEs, solar flares, high-speed solar wind streams, and variations in the strength and direction of IMF [34-36]. Forbush Effects are directly linked to interplanetary disturbances, particularly CMEs and high-speed solar wind streams [11,12,21,37]. When these solar events travel through the interplanetary medium and reach the Earth, they can compress and disturb the Earth's magnetosphere, leading to a reduction in the CR flux. The interaction between the solar wind and the Earth's magnetic field during these disturbances results in the observed FDs. Understanding the relationship between Forbush Effects and interplanetary disturbances is crucial for improving space weather prediction and mitigating the impacts of solar activity on technological systems and human activities in space and on Earth. By analyzing data from multiple solar cycles, researchers can better comprehend the dynamics of these phenomena and develop more accurate models for space weather forecasting. Previous studies have explored the relationship between solar activity and CR modulation, highlighting the role of CMEs and high-speed solar wind streams in modulating CR flux [37,38-40] and the significance of parameters such as maximum IMF intensity (B_{max}) [41], product of solar wind velocity and IMF intensity ($V_m B_m$) [42], and minimum southward IMF component (Bz_{min}) [43]. Understanding these relationships is essential for improving space weather prediction models and mitigating the effects of solar disturbances on technological systems [44,45]. This research aims to build on these studies by providing a comprehensive statistical analysis of these parameters over 23 and 24 solar cycles.

SCs, characterized by an approximately 11-year period, are characterized by alternating periods of solar activity minimum and maximum, during which solar activity fluctuates significantly [46]. Solar cycles 23 and 24, covering the period from 1996 to 2019 [47], provide a rich dataset for analyzing solar-terrestrial interactions. SC 23 spanned from approximately August 1996 to December 2008 and was marked by elevated solar activity, which was followed by SC 24 lasting from December 2008 to December 2019 a period of lower solar activity compared to SC 23 [48-51].

2. DATA COLLECTION AND ANALYSIS

The dataset utilized in this research was acquired from the Forbush Effects and Interplanetary Disturbances database, accessible at http://spaceweather.izmiran.ru/eng/dbs.html, established and meticulously maintained by IZMIRAN [52-54]. This comprehensive database incorporates Forbush Decrease (FD) parameters derived from the global neutron monitor network's data, employing the global survey method for particles with rigidity of 10 GV [55-57]. The global survey method, utilizing data from approximately 40 neutron monitors, enhances the precision of estimating CR density variations and facilitates the differentiation between isotropic and anisotropic components. Sunspot numbers were also obtained from SILSO data/image, Royal Observatory of Belgium, Brussels, accessible at https://www.sidc.be/silso/extheminum [58]. The FEID parameters analyzed include:

- Maximal hourly plasma Beta in the event ($\mathrm{B_{max}}$) - in units of GeV.
- Product of solar wind velocity and Interplanetary Magnetic Field (IMF) intensity in the event ($\mathrm{V_m B_m}$ – in units $\mathrm{kms^{-1}}$nanotesla)
- Minimal hourly Bz component of the IMF enhancements associated with the solar coronal mass ejection in the event ($\mathrm{Bz_{min}}$ - in units of nT).
- The ratio of the minimal hourly Bz component of the IMF to the maximal IMF ($\mathrm{Bz_m to B_m}$)
- The maximal absolute value of the Bz component of the IMF ($\mathrm{ABz_{max}}$).

- FD magnitude for particles with 10 GV rigidity, calculated as maximal range CR density variations in the event ($\boldsymbol{Mag_n}$).
- FD magnitude for particles with 10 GV rigidity, corrected on magnetospheric effect ($\boldsymbol{Mag_n M}$).
- Maximal $\boldsymbol{Kp}$-index in the event ($\boldsymbol{Kp_{max}}$): The $\boldsymbol{Kp}$ -index reflects the global geomagnetic conditions caused by interactions between the solar wind and Earth's magnetosphere [59].
- Minimal $\boldsymbol{Dst}$-index in the event ($\boldsymbol{Dst_{min}}$): The $\boldsymbol{Dst}$-index is a measure of the strength of the disturbance of Earth's magnetosphere caused by variations in the solar wind [60].
- Maximal 3-hour Ap-index in the event ($\boldsymbol{Ap_{max}}$): The Ap-index is another measure of geomagnetic activity that quantifies the planetary-scale magnetic disturbances caused by the interaction between the solar wind and Earth's magnetosphere [61].
- Maximal hourly solar wind speed in the event ($\boldsymbol{V_{max}}$): measure in $\boldsymbol{kms^{-1}}$ is the maximal hourly solar wind speed during an FD event is dependent on the intensity of the interplanetary disturbance, such as ICMEs and high-speed solar wind streams [62].
- The maximum value of the ratio (KT) of the observed hourly average temperature of the solar wind to the temperature, calculated from the velocity of the solar wind ($\boldsymbol{KT_{max}}$): is an important parameter in studying the properties of the solar wind during Forbush Decrease (FD) events.
- Solar sunspot number (SSN): The solar sunspot number is a measure of the number of sunspots on the surface of the Sun. It is calculated using a weighted formula, known as the Wolf sunspot number [63]

These parameters were integrated over each day and averaged over each month to obtain the yearly mean values for the period from 1996 to 2019. Also, Forbush events were grouped based on their Types 1, 2, 3, and 9. Types of Forbush decrease (FD) onset:

- Type 1 – Forbush decrease onset with interplanetary shock waves (ISW) and storm sudden commencement (SSC);
- Type 2 – interplanetary shock wave (ISW)
- Type 3 – weak storm sudden commencement (SSC)
- Type 9 – Forbush decrease onset without interplanetary shock wave (ISW) and storm sudden commencement (SSC)

Types 1 and 9 were observed as dominant Forbush Events that occurred from 1996-2019. From the data, 398 Type 1 Forbush Events and 2271 Type 9 Forbush events were observed. The data were separated according to their respective SCs. The averages were analyzed to identify trends and patterns. OriginLab software was used for all the statistical analysis carried out in this work. To explore the statistical relationships among the parameters, the following statistical tools were employed:

- Descriptive Statistics: Calculation of mean, standard deviation, and other measures of central tendency and dispersion.
- Correlation Analysis: Construction of correlation matrices to examine relationships between parameters
- Time Series Analysis: Tracking annual variations in parameters to identify cyclical patterns linked to solar activity.
- Distribution Plots: Visualization of the frequency distribution of each parameter.

3. RESULTS AND DISCUSSION

The results of yearly average (mean and median) values of FEID parameters for SC 23 and 24 as shown in Table 1 were compared. There was a significant decrease in SSN from SC 23 to SC 24, indicating lower solar activity in SC 24 as reported by [64,65]. Maximum solar wind speed (V_{max}) was higher in SC 23 (mean 526.4 km/s; median 517.7 km/s) than in SC 24 (mean 486.1 km/s; median 475.9 km/s). The yearly average of $Bmax$ shows a similar range of values in SC 23 (mean 12.0 nT; median 12.2 nT) and SC 24 (mean 11.8 nT; median 10.8 nT), suggesting similar values of IMF in both SCs. The yearly average values of the product of solar wind speed and IMF were higher in SC 23 than SC 24 due to higher values of $Vmax$ in SC 23. The values of $Bzmin$ were more negative in SC 23, and $ABzmax$ was higher, pointing towards stronger magnetic disturbances during SC 23. $KTmax$ was higher in SC 23, which could be linked to the higher velocities and magnetic fields.

The yearly average values of both the $Magn$ and $MagnM$ showed a decrease from SC 23 (mean 1.4 and 1.9; median 1.1 and 1.3 respectively) to SC 24, indicating less intense Forbush Events in SC 24. The geomagnetic indices

$Kpmax, Dstmin$ and $Apmax$ were generally higher in SC 23 than in SC 24 indicating intense geomagnetic storms in SC 23 than in SC 24, also noted higher average values of geomagnetic indices in SC 23 than in SC 24.

Also, yearly average values of Type 1 FEID Parameters for SCs 23 and 24 as shown in Table 2 were compared. Both $Vmax$ (SC 23: mean 579.3 km/s, median 586.6 km/s; SC 24: mean 516.9 km/s, median 528.0 km/s) and $Bmax$ (SC 23: mean 17.4 nT, median 15.9 nT; SC 24: mean 15.3 nT, median14.8 nT) as well as their product $VmBm$, (SC 23: mean 5.3, median 4.8; SC 24: mean 4.1, median 4.2) show higher average values in SC 23 compared to SC 24, indicating more intense solar activity in terms of speed and magnetic strength during SC 23 as obtained when all Types of Forbush Event were considered. The yearly average value of the minimum $Bzmin$ was more negative and the absolute maximum $ABzmax$ was higher in SC 23, suggesting more intense fluctuations in the magnetic field during this cycle. The $KTmax$ shows similar KT values in SCs 23 and 24 reflecting potentially similar significant solar activity during this cycle associated with the Type 1 Forbush Effect. The yearly average values of $MagnM$ and $Magn$ are significantly higher in SC 23, suggesting more intense solar activity in terms of strength and magnitude leading to the occurrence formation of the Type 1 Forbush Effect. $Kpmax$ and $Apmax$ show higher maximum Kp and Ap values in SC 23 reflect more intense geomagnetic disturbances compared to SC 24. $Dstmin$ shows less negative value in SC 24 which indicates fewer intense geomagnetic storms compared to SC 23. Both $Axym$ and $Azrange$ are higher in SC 23, indicating more variability and broader spatial impact of geomagnetic disturbances during this cycle.

Similarly, average values of Type 9 FEID parameters for SCs 23 and 24 shown in Table 3 were compared. $Vmax, Bmax, and\ VmBm$ are higher in SC 23, indicating more intense solar activity in terms of speed and interplanetary magnetic field strength during SC 23. $Bzmin$ is slightly less negative in SC 24, and $ABzmax$ is also lower, suggesting less intense fluctuations in the magnetic field during SC 24. SC 23 shows a higher $KTmax$ average value, reflecting potentially more significant solar wind turbulence during this cycle. The average values of $Magn$ and $MagnM$ are slightly higher in SC 23, suggesting a more intense effect of the solar activity events in that cycle. Both $Kpmax$ and $Apmax$ were higher in SC 23, reflecting more intense geomagnetic activity during this solar cycle. The minimum Dst was more negative in SC 23, indicating more intense geomagnetic storms during this cycle compared to SC 24.

Types 1 and 9 FEID parameters across SCs 23 and 24 were compared. The average values of the studied FEID parameters of Type 1 onset event were generally higher than Type 9 onset event during both SCs, indicating that FD onset with interplanetary shock waves (ISW) and storm sudden commencement (SSC) are generally more intense and of greater effect to the space weather than FD onset without ISW and SSC. Log-log plots of the average values of some of the FEID parameters against SSN to check the relationship between them were carried out. Fig. 1a shows the scatter plot of the logarithm of $Bmax$ against the logarithm of SSN, during SCs 23 and 24. For SC 23, the Pearson correlation coefficient r = 0.9 indicates a strong positive correlation between $Bmax$ and SSN. During SC 24, the r = 0.4 suggests a weak positive correlation between $Bmax$ and SSN.

Fig. 1b shows the scatter plot of the logarithm of $Bzmin$ against the logarithm of SSN, during SCs 23 and 24. For SC 23, the correlation coefficient r = 0.9 suggests a strong positive correlation between $Bzmin$ and SSN. The result indicates that there is a strong relationship between the minimum value of the interplanetary magnetic field $Bzmin$ and SSN during SC 23. For SC 24, r = 0.4 suggests a weaker correlation between $Bzmin$ and SSN during SC 24.

Fig. 1c shows the scatter plot of the logarithm yearly mean values of $BzmtoBm$ against the logarithm of the yearly mean values of SSN, during SCs 23 and 24. During SC 23, there is a negative correlation between $BzmtoBm$ and SSN with r = -0.2. This suggests seemly implies a very weak inverse relationship between the two variables during SC 23. On the other hand, during SC 24, there was no correlation between $BzmtoBm$ and SSN with r = 0.1.

Fig. 1d shows the scatter plot of the logarithm of $VmBm$ against the logarithm of SSN during SCs 23 and 24. For SC 23, r = of 0.7 between $VmBm$ and SSN, which suggests a strong relationship. During SC 24, r is 0.2. This value indicates a weaker positive relationship.

Fig. 1e shows the scatter plot of the logarithm of $ABzmax$ against the logarithm of SSN, during

SCs 23 and 24. For SC 23, r = 0.9 and SC 24, r =0.7, these suggest that a strong direct relationship exists between $ABzmax$ and SSN.

Fig. 2a shows the scatter plot for Type 1 mean values of the logarithm of $Bmax$ against the logarithm of SSN, during SSNs 23 and 24. The correlation between $Bmax$ and SSN shows a strong positive relationship during SCs 23 (r = 0.7) & 24 (r =0.8).

Fig. 2b shows the scatter plot for Type 1 mean values of the logarithm of $Bzmin$ against the logarithm of SSN, during SCs 23 and 24. The correlation between them is strong during both SCs 23 (r = 0.8) and 24 (r = 0.6).

Fig. 2c shows the scatter plot for Type 1 mean values of the logarithm of $BzmtoBm$ against the logarithm of SSN, during SCs 23 and 24. The correlation between $BzmtoBm$ and SSN is positive during both SCs, with r = 0.4 in each cycle.

Fig. 2d shows the scatter plot for Type 1 mean values of the logarithm of $VmBm$ against the logarithm of SSN during SCs 23 and 24. The correlation between $VmBm$ and SSN shows a positive relationship during both SCs with, r = 0.6 and 0.7 for SCs 23 and 24 respectively.

Fig. 2e shows the scatter plot for Type 1 mean values of the logarithm of $ABzmax$ against the logarithm of SSN, during SCs 23 and 24. The correlation between $ABzmax$ and SSN is strong during both SCs, with r =0.8. This indicates a positive relationship between the two variables, suggesting that as one variable increases, the other tends to increase as well.

Fig. 3a shows the scatter plot for Type 9 mean values of the logarithm of $Bmax$ against the logarithm of SSN, during SCs 23 and 24. The correlation between $Bmax$ and SSN during SC 23 was found to be strong, with r = 0.8, but slightly weaker during SC 24, with r = 0.6.

Fig. 3b shows the scatter plot for Type 9 mean values of the logarithm of $Bzmin$ against the logarithm of SSN, during SCs 23 and 24. The correlation between $Bzmin$ and SSN is strong during both SCs 23 and 24, with r = 0.8 for cycle 23 and 0.7 for cycle 24. This indicates a positive linear relationship between the $Bzmin$ and sunspot activity during these solar cycles.

Fig. 3c shows the scatter plot for Type 9 mean values of the logarithm of $BzmtoBm$ against the logarithm of SSN, during SCs 23 and 24. During SC 23, the correlation coefficient was 0.4, suggesting a moderate positive correlation between the two variables. In SC 24, the correlation coefficient increased to 0.5, indicating a stronger positive correlation during this period.

Fig. 3d shows the scatter plot for Type 9 mean values of the logarithm of $VmBm$ against the logarithm of SSN during SCs 23 and 24. The correlation analysis between $VmBm$ and SSN reveals a positive association during both SCs 23 and 24. The correlation coefficient r is 0.3 for cycle 23 and 0.3 for cycle 24. These coefficients suggest a moderate positive relationship.

Fig. 3e shows the scatter plot for Type 9 mean values of the logarithm of $ABzmax$ against the logarithm of SSN during SCs 23 and 24. The correlation between $ABzmax$ and SSN is moderately strong, with a correlation coefficient of 0.7 for cycle 23 and 0.6 for cycle 24. This suggests a positive relationship between the $ABzmax$ and the sunspot numbers during these solar cycles. The coefficients indicate that as one variable increases, the other tends to increase as well, demonstrating a statistically significant association between the two parameters.

In Fig. 4(a) shows the time series graph of mean $Bmax$ for SCs 23 and 24. SC 23 generally exhibits a lower $Bmax$ values, whereas cycle 24 shows higher overall strength. These variations reflect the dynamic nature of solar activity affecting different cycles. Fig. 4(b) shows the time series graph of mean values of $Bzmin$ for SCs 23 and 24. In solar cycle 23, $Bzmin$ values range from -8.1 to -5.6, indicating a notable range. Solar cycle 24 exhibits a slightly wider range, from -7.0 to 2.1. The trend in cycle 23 generally shows a decreasing pattern, while cycle 24 displays a mix of negative and positive values, suggesting a less consistent trend. Fig. 4(c) shows the time series graph of mean values of $BzmtoBm$ for SCs 23 and 24. In solar cycle 23, values range from 0.6 to 0.7, while in solar cycle 24, the range is wider, from 0.6 to 5.9. This indicates a more diverse and pronounced behavior of the interplanetary magnetic field during Forbush events in cycle 24 compared to cycle 23. Fig. 4(d) shows the time series of mean $VmBm$ values for SCs 23 and 24. In cycle 23, values ranged from 2.4 to 4.3, while in cycle 24, they varied more widely from 1.9 to 8.9. Cycle 23 shows a general increase in $VmBm$, whereas cycle 24 exhibits irregular fluctuations. These differences highlight the dynamic and complex interactions between solar wind and magnetic field intensity across the cycles. Fig. 4(e) shows the time series graph of mean values of $ABzmax$ for SCs 23 and 24. For SC 23, values range from 5.9 to 9.8, while SC 24 ranges from 4.9 to 8.4. Analyzing the trends, $ABzmax$ generally show an increasing pattern from the beginning to the middle of the cycles, with some fluctuations.

In general, there is a consistent spike in the values of the parameters relenting to IMF during the 3rd year of SC 24, indicating strong magnetic disturbances in the 3rd year of SC 24. Throughout 2011, several geomagnetic storms were recorded, which were likely associated with significant southward (negative) Bz components. For instance, major geomagnetic storms in August 2011 and September 2011 were linked to coronal mass ejections (CMEs) that interacted with Earth's magnetosphere.

These storms were characterized by sustained negative Bz values, sometimes reaching extreme levels. Specifically, in August 2011, a strong geomagnetic storm occurred, triggered by a CME that resulted in a significant negative Bz. This event was associated with strong auroras and disrupted communications, also, in September 2011, another geomagnetic storm was recorded, again associated with a negative Bz component following a CME. This period saw sustained southward Bz values, leading to notable geomagnetic disturbances.

Fig. 5(a & b) shows the time series graph of Types 1 and 9 mean $Bzmin$ in the event SCs 23 and 24. For cycle 23, Type 1 events exhibit $Bzmin$ values ranging from -6.4 to -13.8, indicating higher geomagnetic disturbances. Type 9 events range from -4.8 to -6. 5. During cycle 24, Type 1 events show a consistent downward trend in $Bzmin$ values, from -6.49 in the first year to -11.75 in the eighth year, while Type 9 events display a less pronounced downward trend, ranging from -4.47 to -6.36. Fig. 5(c & d) shows the time series graph of Types 1 and 9 means of the ratio of the minimal hourly Bz component of the IMF to the maximal IMF ($BzmtoBm$) for SCs 23 and 24. For SC 23, Type 1 events display a fluctuating $BzmtoBm$ ratio, reflecting the dynamic nature of these events. Type 9 events show a relatively steady increase in the $BzmtoBm$ ratio, suggesting a possible correlation with specific solar cycle dynamics. During solar cycle 24, Type 1 events exhibit a fluctuating $BzmtoBm$ ratio, ranging from 0.6 in year 1 to 0.8 in year 12. In contrast, Type 9 events demonstrate a more stable trend with less pronounced variability in the $BzmtoBm$ ratio, ranging from 0.6 in year 1 in year 11 to 0.7 in year 6. Fig. 5(e & f) shows the time series graph of type 1 and 9 mean of $ABzmax$ (maximal absolute value of the Bz component of the Interplanetary Magnetic Field) for SCs 23 and 24. For SC 23, Type 1 events exhibit a general increasing trend in $ABzmax$, peaking around year 8, followed by a decrease. Type 9 events display fluctuating $ABzmax$ values with no clear trend. During SC 24, Type 1 events show an increase in $ABzmax$ values from the initial years, peaking around year 4, then gradually declining. Type 9 events maintain a more stable but lower magnitude of $ABzmax$ values throughout the cycle.

Fig. 6(a & b) shows the time series graph of type 1 and 9 mean $Bmax$ (maximal hourly IMF intensity in the event) for SCs 23 and 24. For SC 23, Type 1 events show a lower mean value of around 13.16 initially, peaking at 25.05 in year 8, then declining, indicating complex influences. Type 9 events have generally lower $Bmax$ values, ranging from 9.1 to 12.1, peaking in year 8, similar to Type 1 events. During SC 24, Type 1 events display an increasing pattern in $Bmax$ values, peaking in the fourth year, followed by a decrease, while Type 9 events maintain a relatively stable trend with minor fluctuations. Fig. 6(c & d) shows the time series graph of Types 1 and 9 yearly mean values of the normalized product of maximal solar wind speed and IMF strength ($VmBm$) for SCs 23 and 24. In Type 1 events for SC 23, values range from 2.8 in the first year to a peak of 9.3 in the tenth year. Type 9 events fluctuate throughout the cycle, ranging from 2.1 in the 2nd year to 3.9 in the eighth year. During SC 24, Type 1 events show a fluctuating pattern, ranging from 1.9 in the second year to 5.8 in the 4th year. Type 9 events also display variability, with values ranging from 1.9 to 3.1.

Fig. 7(a) shows the distribution of $Bmax$, with its frequency ranging from 0-1400, and it shows a highly right-skewed distribution with a skewness of 2.7 and a high kurtosis of 14.5, indicating heavy tails and a very peaked center. Fig. 7(b) shows the distribution of $Bzmin$ which is highly left-skewed with a negative skewness of -3.9 and a high kurtosis of 31.2, indicating heavy tails and a peaked distribution, with its frequency ranging from 0-1300. Fig. 7(c) shows the distribution of $BzmtoBm$, with its frequency ranging from 0-400 and it shows a roughly symmetric distribution with a skewness of 0.1 and a kurtosis of -0.5, indicating lighter tails than a normal distribution.

Table 1. Yearly average values of SSN and FEID parameters

Year	SSN	Vmax	Bmax	VmBm	Bzmin	ABzmax	KTmax	Magn	MagM	Kpmax	Dstmin	Apmax
						Solar Cycle 23						
1996	11.6	503.0	9.8	2.5	-5.0	5.9	4.6	0.9	1.2	3.8	-30.2	29.0
1997	28.9	443.7	10.3	2.4	-5.8	7.0	4.5	0.9	1.4	3.7	-37.2	30.5
1998	88.3	482.9	12.2	3.1	-6.6	8.0	2.7	1.4	1.8	4.1	-55.0	38.5
1999	136.3	517.7	12.4	3.3	-7.0	8.4	2.9	1.5	2.0	4.2	-41.9	39.0
2000	173.9	522.2	13.8	3.9	-7.8	9.2	2.6	1.8	2.5	4.4	-51.5	49.0
2001	170.4	507.5	14.3	3.9	-8.1	9.8	2.6	1.9	2.7	4.3	-52.2	45.3
2002	163.6	516.7	13.6	3.6	-7.1	8.7	2.7	1.7	2.4	4.3	-49.7	40.5
2003	99.3	639.8	13.4	4.3	-7.2	8.6	2.4	1.8	2.4	5.1	-53.7	60.4
2004	65.3	535.3	11.9	3.4	-6.8	7.7	2.7	1.4	1.9	4.2	-47.2	42.2
2005	45.8	557.9	12.9	3.9	-7.1	8.6	2.8	1.6	2.1	4.4	-49.3	47.5
2006	24.7	508.9	10.6	2.9	-5.7	6.6	2.7	1.1	1.4	3.7	-29.0	31.6
2007	12.6	536.5	10.7	3.0	-5.6	6.8	2.9	0.9	1.3	3.7	-24.0	26.4
2008	4.2	571.7	10.1	3.0	-5.4	6.6	2.9	1.1	1.5	3.7	-27.7	27.0
Mean	78.8	526.4	12.0	3.3	-6.6	7.8	3.0	1.4	1.9	4.1	-42.2	39.0
Median	65.3	517.7	12.2	3.3	-6.8	8.0	2.7	1.4	1.9	4.2	-47.2	39.0
Year						**Solar Cycle 24**						
2008	4.2	571.7	10.1	3.0	-5.4	6.6	2.9	1.1	1.5	3.7	-27.7	27.0
2009	4.8	430.1	8.6	1.9	-4.9	5.7	2.7	0.8	1.1	2.8	-17.8	15.3
2010	24.9	464.6	21.3	8.9	2.1	-4.8	0.7	0.7	0.9	55.3	21.0	3.1
2011	80.8	485.2	10.0	2.6	-5.3	6.4	3.0	1.1	1.6	3.3	-27.1	24.8
2012	84.5	470.1	10.7	2.6	-6.3	7.4	3.0	1.4	1.8	3.7	-33.7	30.2
2013	94.0	471.7	10.6	2.6	-6.3	7.3	2.9	1.4	1.7	3.6	-33.7	28.2
2014	113.3	466.4	10.5	2.5	-5.8	7.4	0.1	1.9	1.8	3.4	-26.3	23.3
2015	69.8	520.4	12.6	3.4	-7.0	8.2		1.3	1.9	4.2	-43.2	
2016	39.8	503.0	11.3	2.9	-5.9	7.1	2.3	1.1	1.1	3.7	-28.9	27.9
2017	21.7	523.4	10.0	2.8	-5.1	6.0	2.4	0.9	0.9	3.6	-26.1	27.9
2018	7.0	480.1	9.2	2.3	-4.7	5.4	2.1	0.7	0.7	3.2	-22.1	22.0
2019	3.6	445.9	8.2	1.9	-4.2	4.9	1.9	0.6	0.6	3.0	-16.0	18.1
Mean	45.7	486.1	11.8	3.1	-4.9	5.6	2.2	1.1	1.3	3.6	-23.5	22.5
Median	32.4	475.9	10.8	2.6	-5.4	6.5	2.4	1.1	1.3	3.6	-26.7	24.8

Table 2. Yearly Average Values of Type 1 FEID Parameters

Year	Vmax	Bmax	VmBm	Bzmin	ABzmax	KTmax	Magn	MagM	Kpmax	Dstmin	Apmax
						Solar Cycle 23					
1996	454.5	12.3	2.8	-6.8	8.2	5.7	0.7	1.2	4.1	-22.5	30.0
1997	476.1	14.8	3.6	-10.1	11.7	5.5	1.3	2.6	5.2	-70.3	66.3
1998	518.9	15.9	4.2	-9.0	11.0	2.8	2.1	2.7	5.3	-76.2	63.5
1999	535.7	14.5	4.8	-10.0	12.0	3.3	2.0	3.1	5.3	-63.2	69.7
2000	592.1	19.7	6.2	-11.1	12.9	2.5	3.1	4.6	5.8	-81.2	88.3
2001	578.1	22.1	7.0	-12.7	15.6	2.8	4.1	5.5	5.6	-90.8	90.9
2002	517.8	18.7	5.1	-9.7	11.5	3.1	3.0	4.1	5.5	-65.7	70.0
2003	666.3	25.1	7.3	-11.6	17.3	2.3	3.9	4.9	6.7	-112.0	148.9
2004	608.8	20.4	6.7	-12.4	14.1	3.1	3.4	4.6	5.2	-86.3	89.8
2005	690.8	24.2	9.2	-13.8	15.4	3.4	4.3	6.1	5.9	-98.1	113.4
2006	631.7	12.7	4.2	-6.4	7.1	2.5	2.6	3.3	5.0	-47.1	65.3
2007	673.2	14.0	4.7	-7.0	8.8	3.8	1.1	1.9	4.7	-41.3	42.7
2008	586.6	11.8	3.5	-6.5	6.6	3.5	1.3	1.9	3.9	-26.7	25.9
Mean	**579.3**	**17.4**	**5.3**	**-9.8**	**11.7**	**3.4**	**2.5**	**3.6**	**5.3**	**-67.8**	**74.2**
Median	**586.6**	**15.9**	**4.8**	**-10.0**	**11.7**	**3.1**	**2.6**	**3.3**	**5.3**	**-70.3**	**69.7**
Year						**Solar Cycle 24**					
2008	586.6	11.8	3.5	-6.5	6.6	3.5	1.3	1.9	3.9	-26.7	25.9
2009	422.0	9.2	1.9	-4.6	5.5	2.5	0.9	1.2	3.0	-16.0	17.4
2010	510.7	12.8	3.4	-7.2	9.4	3.0	1.5	2.4	4.8	-46.4	60.6
2011	540.6	20.4	5.8	-10.0	13.9	4.6	2.9	3.9	5.3	-55.1	72.4
2012	515.4	18.4	4.9	-11.2	13.0	3.7	3.3	4.2	5.2	-72.0	70.3
2013	558.9	14.6	4.2	-8.2	9.7	3.3	2.5	3.2	5.0	-56.9	-0.6
2014	497.5	14.9	3.9	-6.8	11.0	0.1	3.4	3.2	4.1	-31.0	28.3
2015	554.8	19.3	5.6	-11.8	12.4		2.4	3.6	5.7	-78.3	
2016	467.4	20.0	4.8	-10.1	12.1	2.0	1.7	1.8	4.9	-58.0	56.0
2017	607.4	16.7	5.2	-10.3	10.6	4.9	2.0	2.1	5.3	-53.8	70.2
2018	564.8	14.2	4.1	-7.5	8.8	3.4	0.9	1.0	4.5	-33.5	39.9
2019	377.0	11.9	2.2	-8.4	9.3	2.4	1.1	1.4	3.3	-16.0	18.0
Mean	**516.9**	**15.3**	**4.1**	**-8.5**	**10.2**	**3.0**	**2.0**	**2.5**	**4.6**	**-45.3**	**41.7**
Median	**528.0**	**14.8**	**4.2**	**-8.3**	**10.2**	**3.3**	**1.9**	**2.3**	**4.9**	**-50.1**	**39.9**

Table 3. Yearly average values of Type 9 FEID parameters

	Vmax	Bmax	VmBm	Bzmin	ABzmax	KTmax	Magn	MagM	Kpmax	Dstmin	Apmax
Year						**Solar Cycle 23**					
1996	505.1	9.5	2.4	-4.8	5.6	4.5	0.9	1.2	3.7	-30.9	29.0
1997	436.4	9.0	2.0	-4.8	5.5	4.3	0.8	1.1	3.3	-28.9	21.4
1998	465.3	10.7	2.6	-5.9	6.9	2.6	1.2	1.5	3.7	-47.2	28.7
1999	511.1	11.8	2.8	-6.0	7.2	2.8	1.3	1.5	3.8	-33.6	28.8
2000	483.4	10.9	2.7	-6.1	7.3	2.6	1.1	1.5	3.7	-34.4	27.5
2001	479.2	11.4	2.8	-6.3	7.7	2.6	1.1	1.6	3.7	-36.4	27.6
2002	515.8	12.0	3.2	-6.3	7.7	2.6	1.3	1.9	3.9	-43.8	31.6
2003	631.0	12.1	3.9	-6.5	7.5	2.4	1.3	1.9	4.9	-45.2	49.7
2004	5210	10.5	2.8	-5.8	6.5	2.7	1.0	1.3	4.0	-36.1	30.5
2005	5411	11.2	3.2	-6.0	7.4	2.8	1.1	1.5	4.1	-40.0	34.9
2006	4993	10.2	2.7	-5.7	6.5	2.6	0.9	1.2	3.6	-27.2	27.8
2007	5301	10.3	2.9	-5.5	6.5	2.8	0.9	1.3	3.6	-23.5	25.9
2008	5547	9.4	2.7	-5.0	6.3	2.7	0.9	1.3	3.6	-26.8	25.2
Mean	**5134**	**10.7**	**2.8**	**-5.7**	**6.8**	**2.9**	**1.1**	**1.5**	**3.8**	**-34.9**	**29.9**
Median	**5111**	**10.7**	**2.8**	**-5.9**	**6.9**	**2.7**	**1.1**	**1.5**	**3.7**	**-34.4**	**28.7**
Year						**Solar Cycle 24**					
2008	554.7	9.4	2.7	-5.0	6.3	2.7	0.9	1.3	3.6	-26.8	25.2
2009	431.4	8.4	1.9	-4.8	5.6	2.7	0.8	1.1	2.8	-17.3	14.6
2010	461.1	8.5	2.0	-4.6	5.6	2.7	0.8	1.1	2.9	-21.1	17.1
2011	474.8	8.7	2.1	-4.7	5.5	2.8	0.9	1.3	3.0	-22.9	15.9
2012	461.7	9.4	2.2	-5.5	6.5	2.8	1.1	1.4	3.5	-26.8	23.4
2013	456.6	9.9	2.3	-6.0	6.9	2.9	1.2	1.5	3.4	-29.7	23.6
2014	459.2	9.5	2.2	-5.5	6.6	0.1	1.5	1.5	3.3	-25.0	21.7
2015	512.1	11.6	3.0	-6.4	7.4		1.1	1.6	4.0	-37.2	
2016	503.3	10.8	2.8	-5.6	6.9	2.3	1.1	1.1	3.6	-26.9	26.5
2017	511.6	9.1	2.4	-4.5	5.4	2.1	0.8	0.8	3.4	-22.7	22.5
2018	474.8	8.7	2.1	-4.5	5.1	1.9	0.7	0.7	3.1	-21.4	20.6
2019	447.1	8.1	1.9	-4.1	4.9	1.9	0.6	0.6	3.0	-15.9	17.8
Mean	**479.0**	**9.3**	**2.3**	**-5.1**	**6.0**	**2.3**	**1.0**	**1.2**	**3.3**	**-24.5**	**20.8**
Median	**468.3**	**9.3**	**2.2**	**-4.9**	**6.0**	**2.7**	**0.9**	**1.2**	**3.4**	**-24.0**	**21.7**

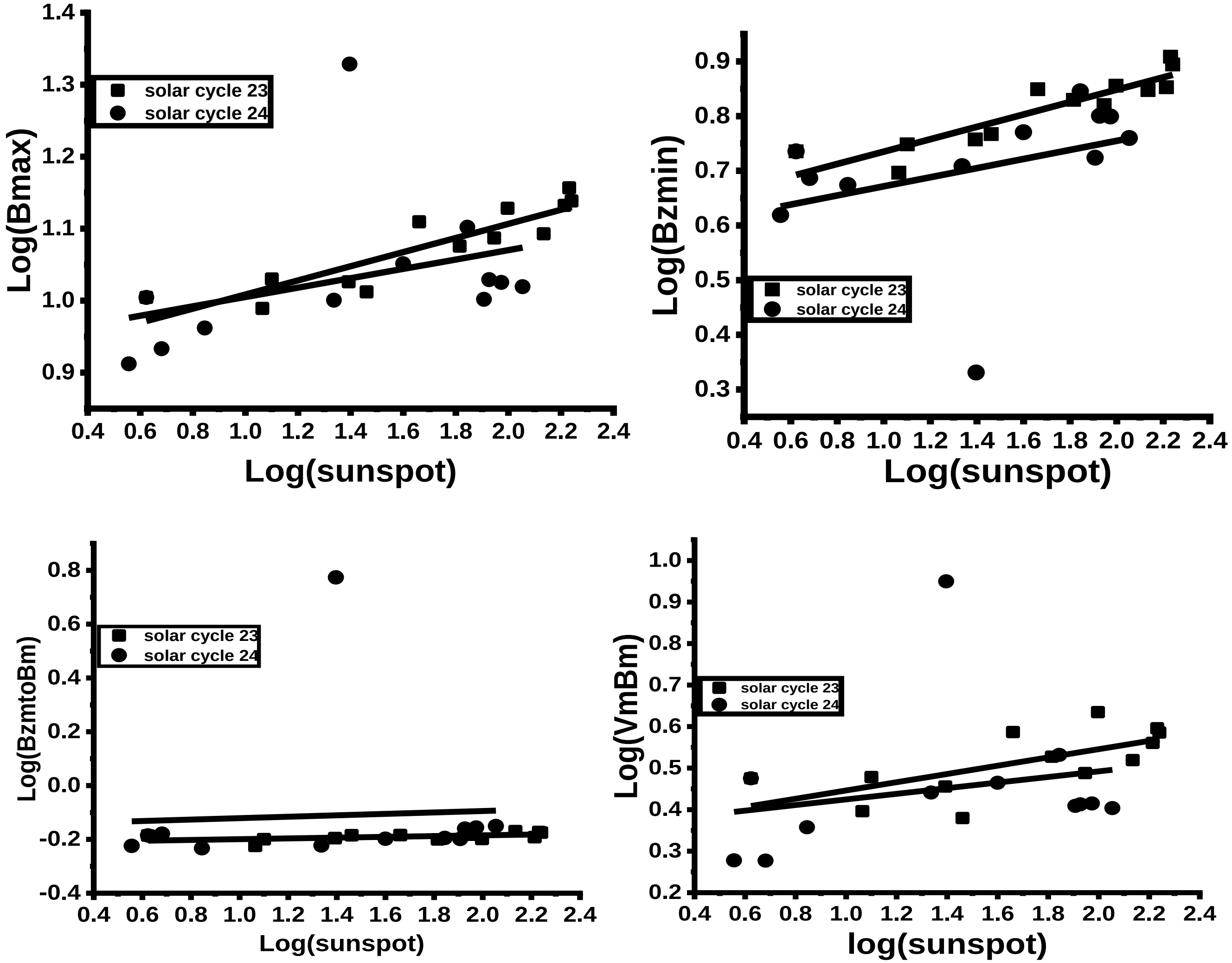
Log(Bmax)
solar cycle 23
solar cycle 24
Log(sunspot)
Log(Bzmin)
solar cycle 23
solar cycle 24
Log(sunspot)
Log(BzmtoBm)
solar cycle 23
solar cycle 24
Log(sunspot)
Log(VmBm)
solar cycle 23
solar cycle 24
log(sunspot)

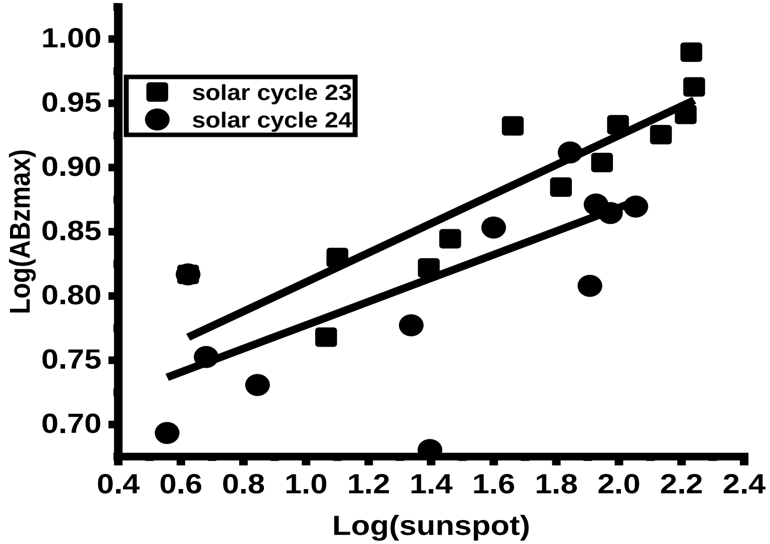

Fig. 1(a-e from top left to bottom). Log-log Scatter Plots of Mean values of (a) $Vmax$, (b) $VmBm$, (c) $Bmax$ and (d) $Bzmin$ (e) $ABzmax$ for all events for SCs 23 & 24 against Yearly Mean values SSN

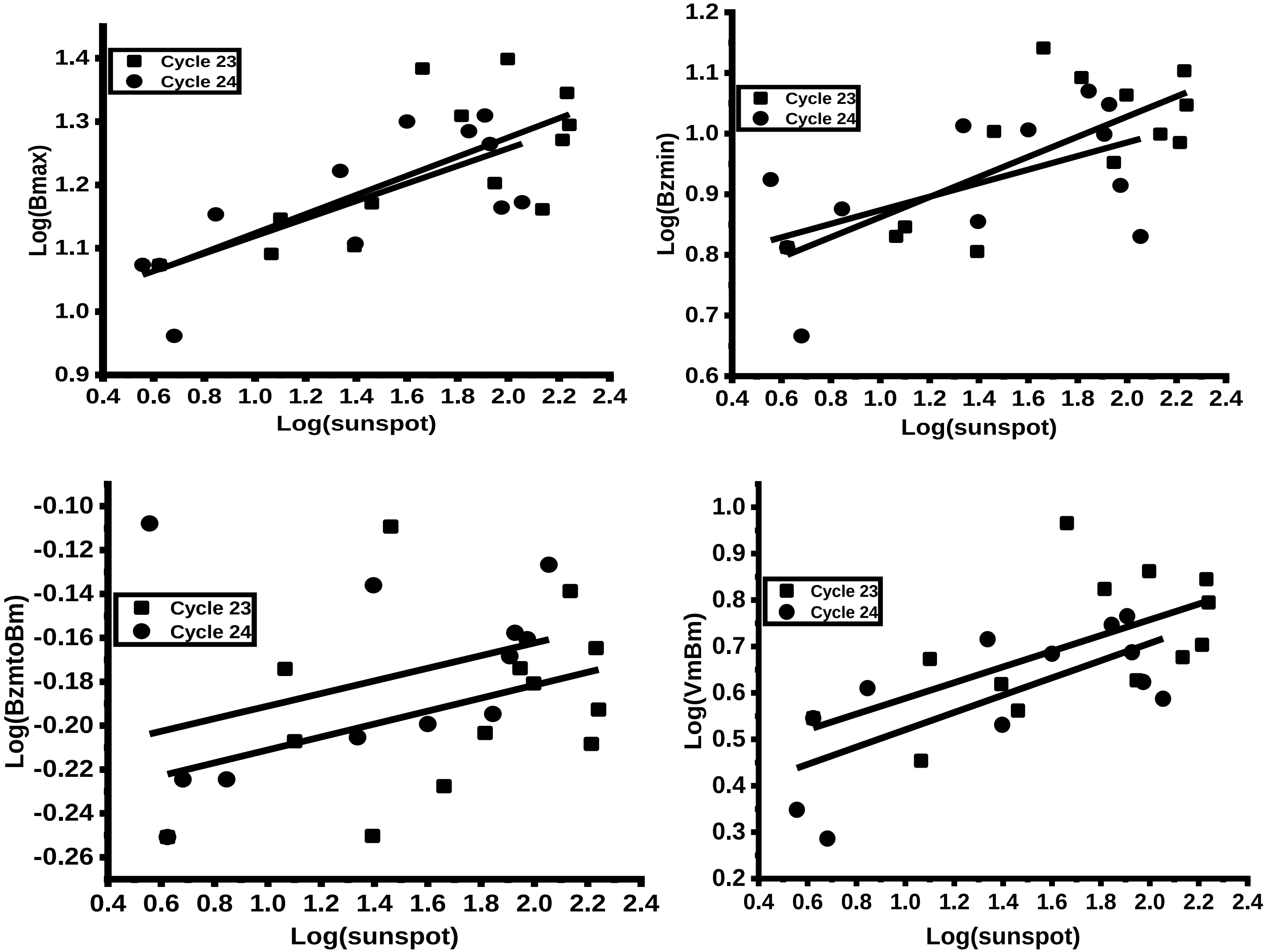
Cycle 23
Cycle 24
Log(Bmax)
Log(sunspot)
Log(Bzmin)
Log(BzmtoBm)
Log(VmBm)

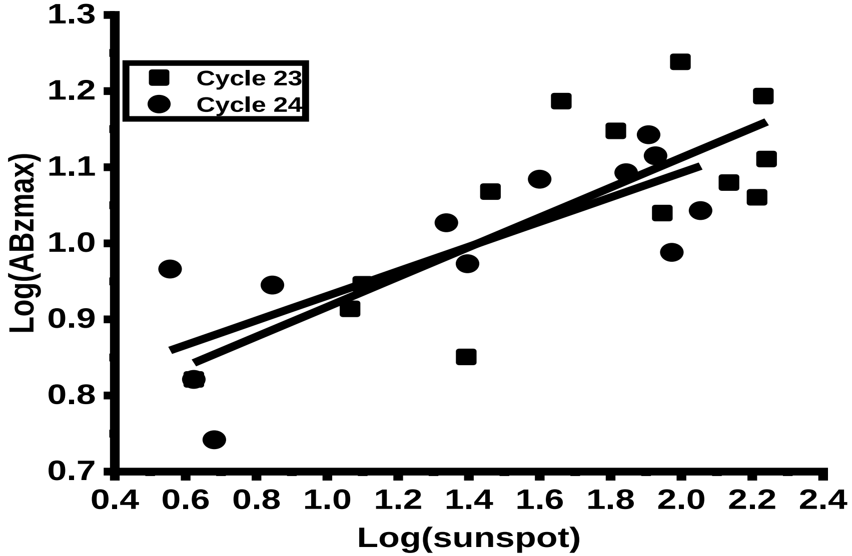

Fig. 2. (a-e) from top left to bottom right). Log-log Scatter Plots of Yearly Mean values of (a) $Vmax$, (b) $VmBm$, (c) $Bmax$ and (d) $Bzmin$ (e) $ABzmax$ for Type 1 events for SCs 23 & 24 against Yearly mean values of SSN

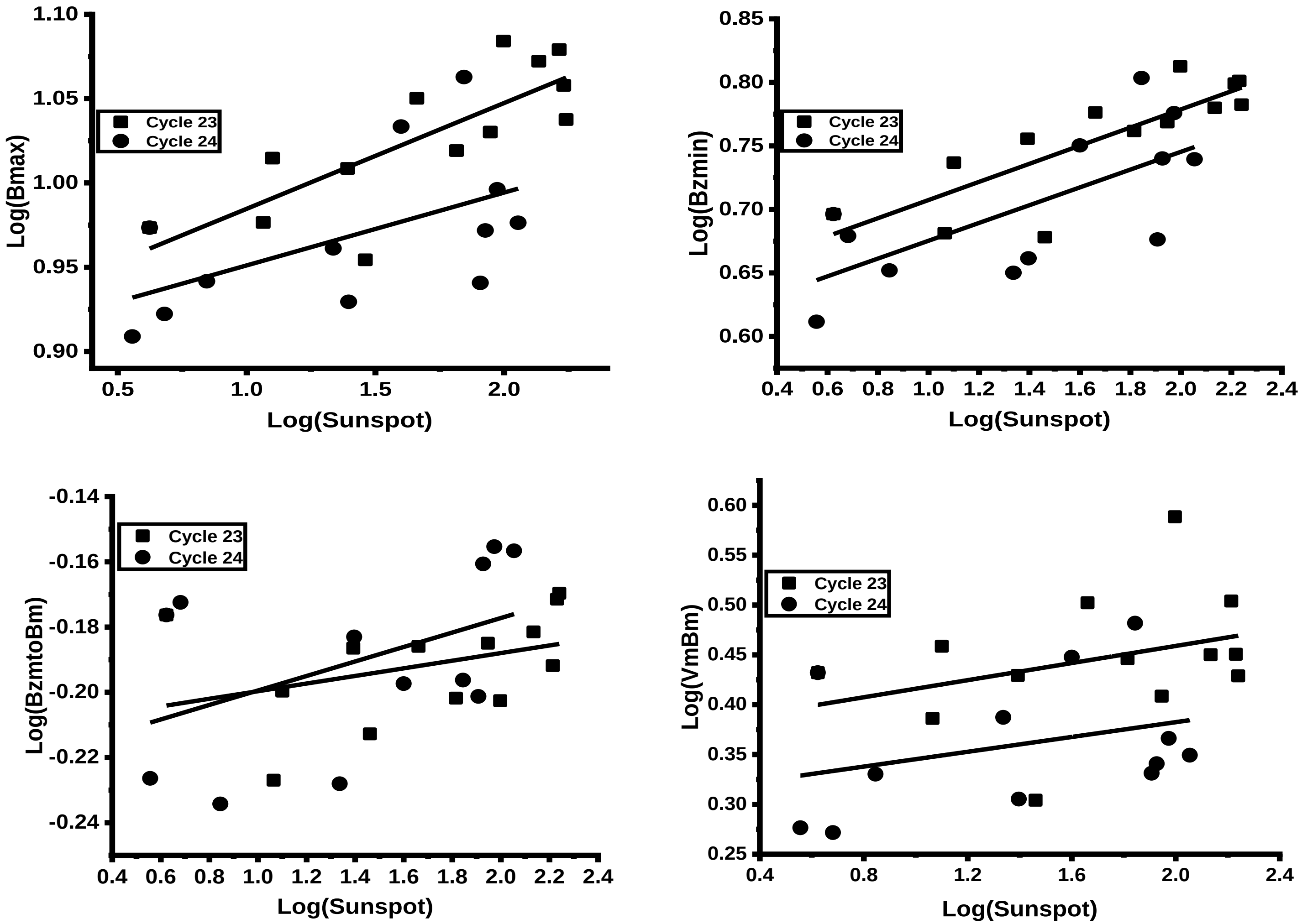
Log(Bmax)
Log(Sunspot)
Cycle 23
Cycle 24
Log(Bzmin)
Log(Sunspot)
Cycle 23
Cycle 24
Log(BzmtoBm)
Log(Sunspot)
Cycle 23
Cycle 24
Log(VmBm)
Log(Sunspot)
Cycle 23
Cycle 24

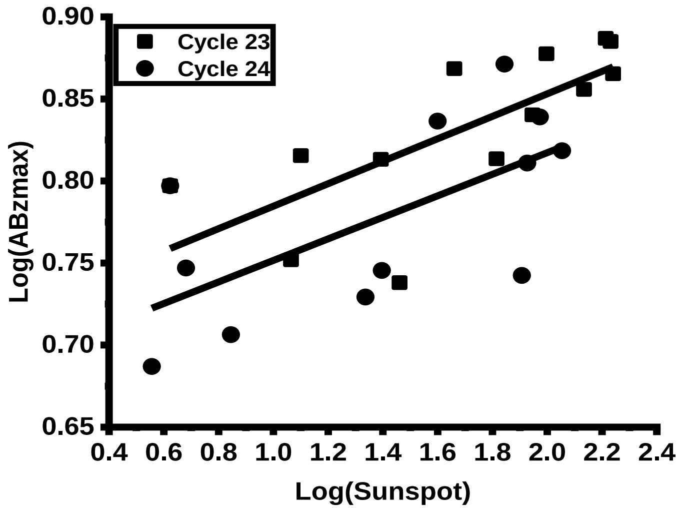

Fig. 3. (a-e from top left to bottom). Log-log Scatter Plots of Yearly Mean values of (a) $Vmax$, (b) $VmBm$, (c) $Bmax$ and (d) $Bzmin$ (e) $ABzmax$ for Type 9 events for SCs 23 & 24 against Yearly mean values of SSN

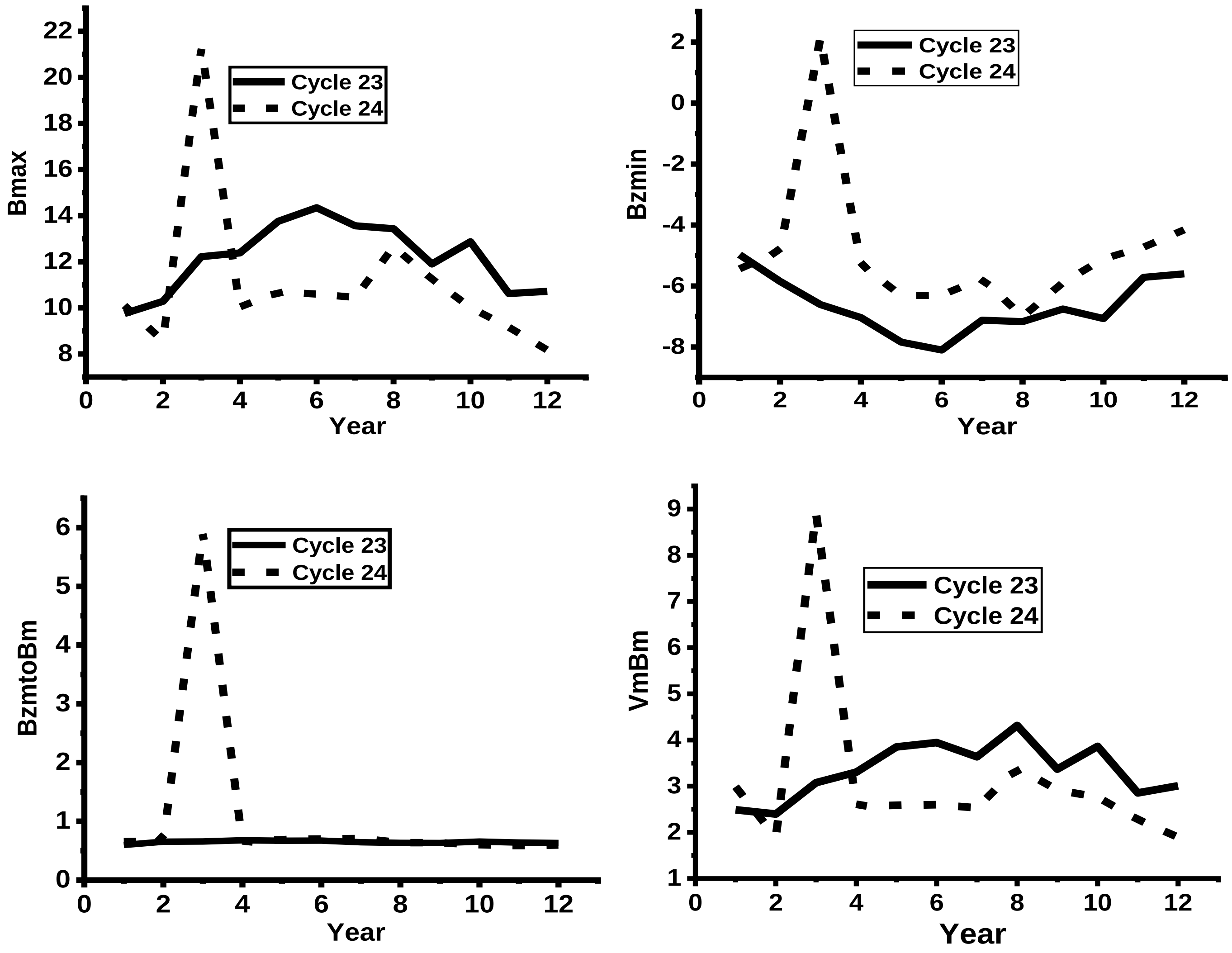
Bmax
Year
Cycle 23
Cycle 24
Bzmin
Year
Cycle 23
Cycle 24
BzmtoBm
Year
Cycle 23
Cycle 24
VmBm
Year
Cycle 23
Cycle 24

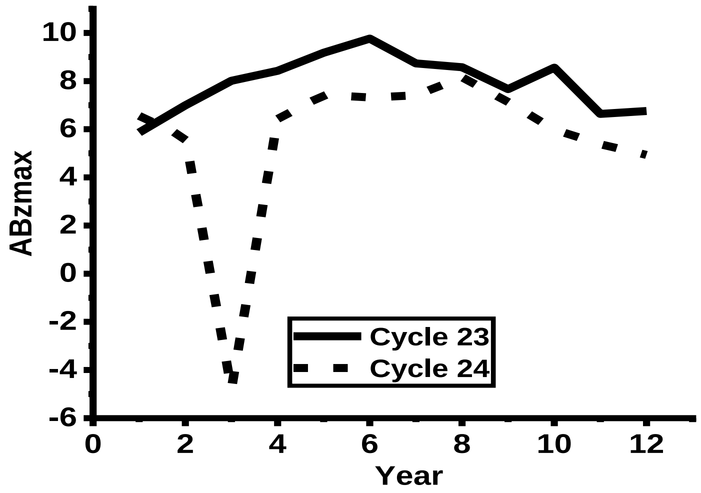

Fig. 4. Time series graph of Yearly Mean of all events (a) $Bmax$, (b) $Bzmin$, (c) $BzmtoBm$ (d) $VmBm$ and (e) $ABzmax$ for cycle 23 and 24

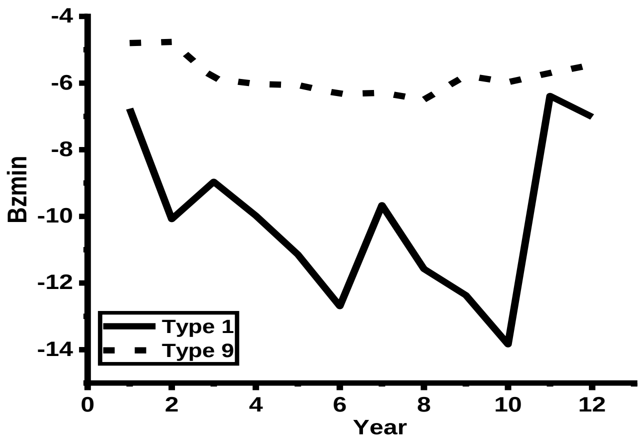

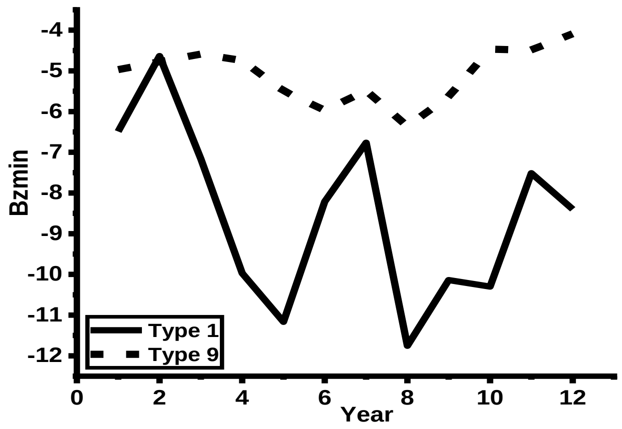

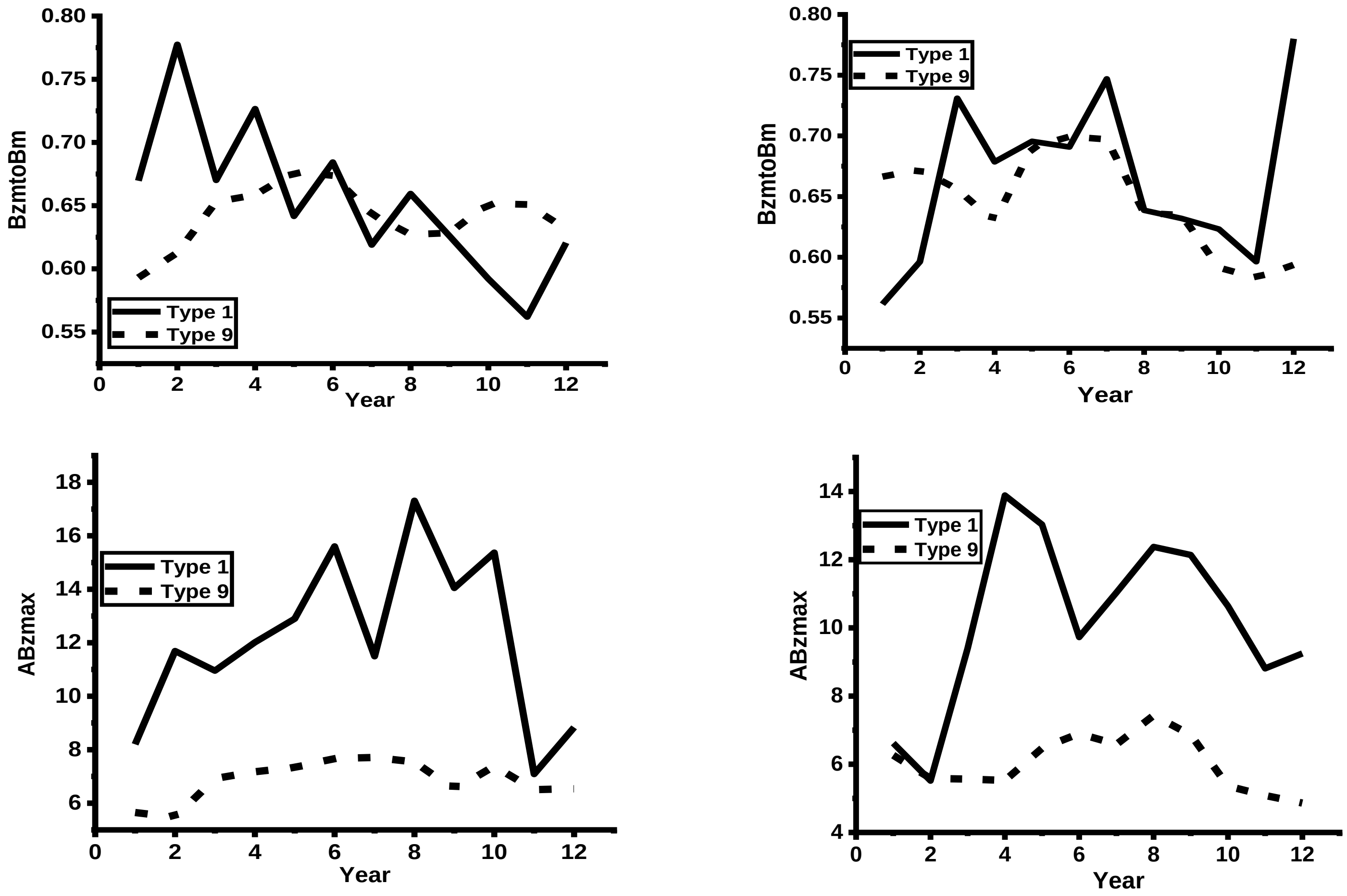

Fig. 5. Time series graph of Yearly Mean (a&b) $Bzmin$ (top), (c&d) $BzmtoBm$ (middle) and (e&f) $ABzmax$ (bottom) for SCs 23 (left) and 24 (right) for Type 1 and Type 9 events

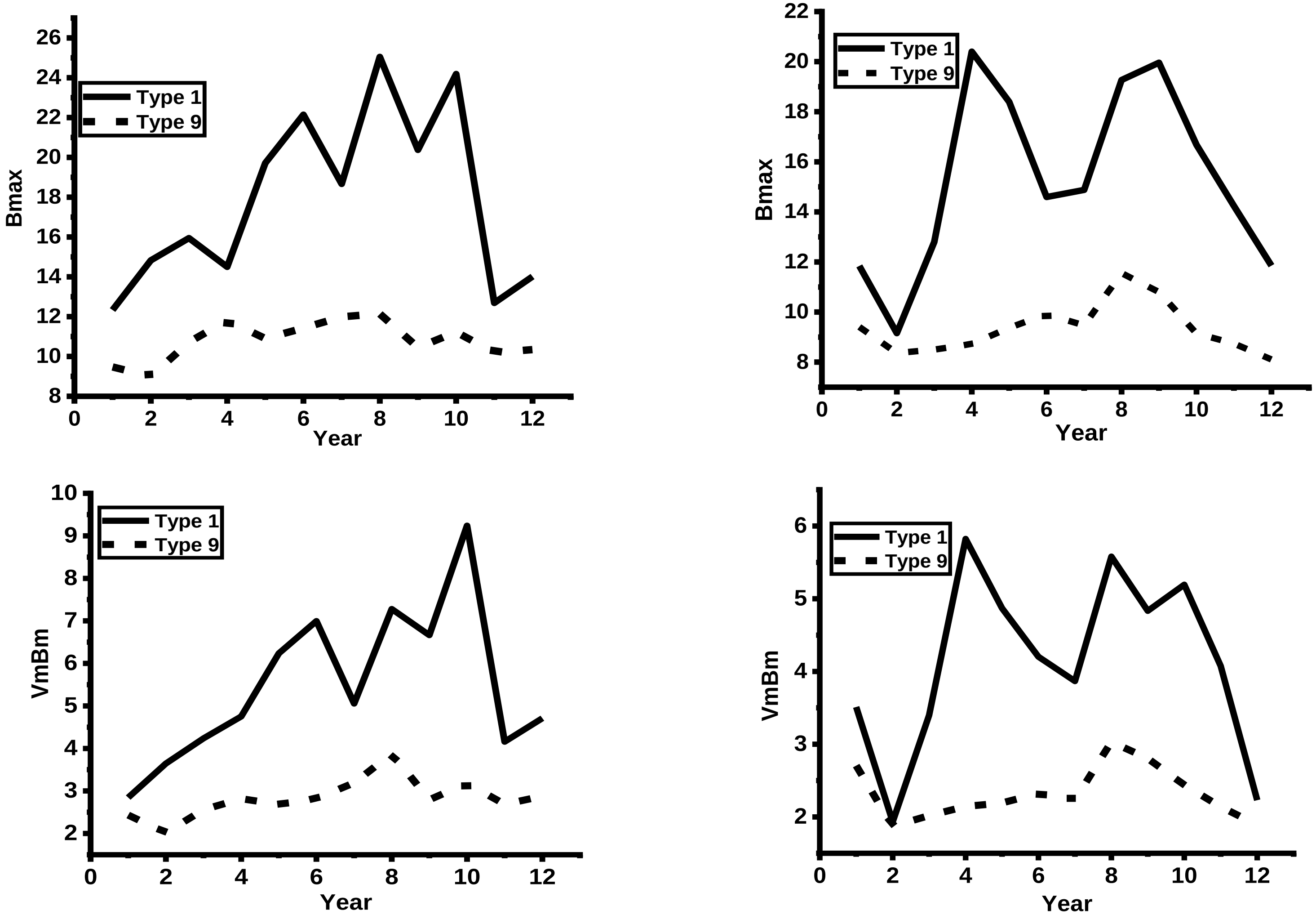

Fig. 6. Time series graph of Yearly Mean (a&b) $Bmax$ (top)and (c&d) $VmBm$ (bottom)for Type 1 and Type 9 events for SCs 23 (left) & 24 (right)

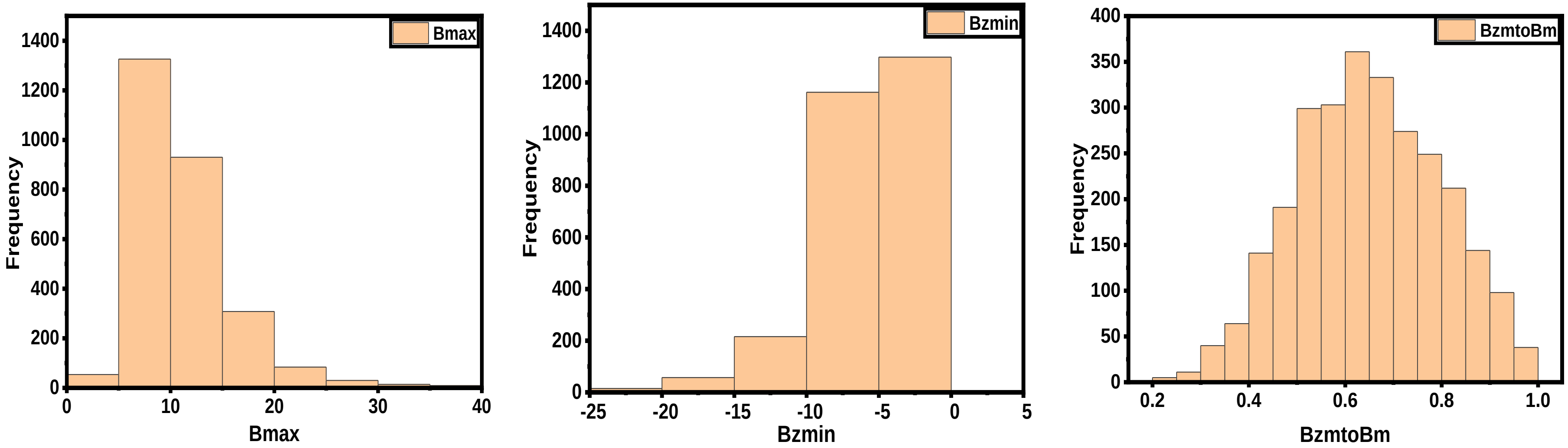
Bmax
Frequency
Bmax
0
200
400
600
800
1000
1200
1400
0
10
20
30
40
Bzmin
Frequency
Bzmin
-25
-20
-15
-10
-5
0
5
BzmtoBm
Frequency
BzmtoBm
0
50
100
150
200
250
300
350
400
0.2
0.4
0.6
0.8
1.0

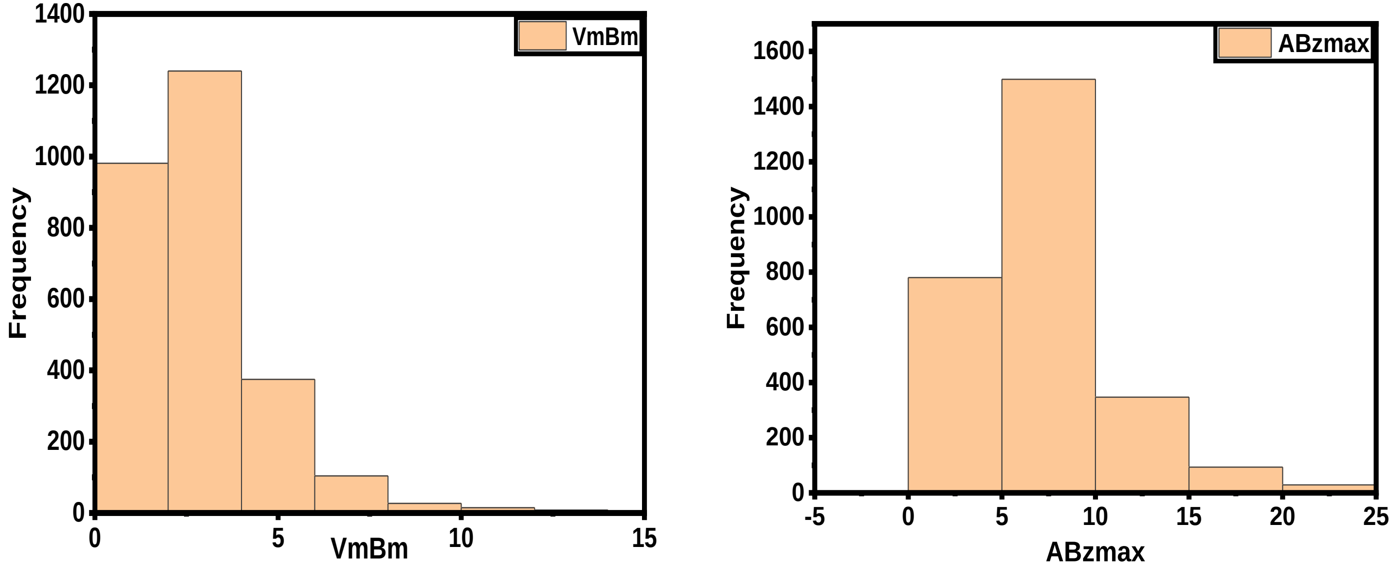

Fig. 7(a-e). Distribution plot of (a) $Bmax$ (b)$Bzmin$, (c) $BzmtoBm$ (d) $VmBm$ (e) $ABzmax$ for all Forbush events

Fig. 7(d) shows the distribution of $VmBm$ shows a highly right-skewed distribution with a skewness of 4.2 and an extremely high kurtosis of 33.9, suggesting heavy tails and a very peaked distribution, with its frequency ranging from 0-1300. Fig. 7(e) shows the distribution of $ABzmax$ which has a right-skewed distribution with a positive skewness of 3.4 and a relatively high kurtosis of 22.5, suggesting heavy tails and a peaked distribution, with its frequency ranging from 0-1500.

4. CONCLUSION

This study provides a comprehensive statistical analysis of Forbush Effects and Interplanetary Disturbances (FIEDs) parameters across solar cycles 23 and 24, spanning from 1996 to 2019. The research focuses on key parameters such as $Bmax,\ VmBm,\ Bzmin$, $BzmtoB$, $Dst,\ KTmax,\ Kpmax,\ Apmax$ and $ABzmax$ using data from 2,669 Forbush events. By employing descriptive statistics, distribution plots, time series analysis, and Pearson correlation coefficients, the study examines the intricate relationships between these parameters. The analysis reveals significant variations and correlations in FEID parameters over both SCs, highlighting the dynamic interactions between solar activity, interplanetary magnetic fields, and cosmic ray intensity variations. For instance, a strong negative correlation was found between $Bmax$ and sunspot numbers during Solar Cycle 23, while a weaker positive correlation was observed in Solar Cycle 24. Similar patterns were noted for $Bzmin$ and sunspot numbers, with Cycle 23 showing a strong relationship and Cycle 24 exhibiting a weaker positive correlation. The findings demonstrate the substantial impact of solar phenomena on space weather, emphasizing the importance of parameters like the Bz component in understanding and predicting these events. The study underscores the complex nature of solar-terrestrial interactions and provides valuable insights into the mechanisms driving Forbush Effects. By extending the analysis to include recent solar cycles and employing advanced statistical techniques, this research enhances our ability to forecast space weather and mitigate its effects on technological systems and human activities. It contributes significantly to the field of solar-terrestrial physics, offering a deeper understanding of FEID parameter behaviors and their implications for space weather prediction and cosmic ray modulation.

DISCLAIMER (ARTIFICIAL INTELLIGENCE)

Author(s) hereby declare that NO generative AI technologies such as Large Language Models (ChatGPT, COPILOT, etc.) and text-to-image generators have been used during the writing or editing of this manuscript.

COMPETING INTERESTS

The authors have declared that no competing interests exist.

REFERENCES

1. Jaisawal M, Chouhan ML, Katare R. The effect of solar and interplanetary disturbance on space weather. International Journal of Creative Research Thoughts. 2023;11(3):b947-b954.
   Available:https://ijcrt.org/papers/IJCRT2303212.pdf
2. Gopalswamy N. The Sun and space weather. Atmosphere. 2022;13(11):1781.
   Available:https://doi.org/10.3390/atmos13111781
3. Georgieva K. Solar influences on the atmosphere and climate. EMS Annual Meeting 2022, Bonn, Germany. 5–9 September 2022;EMS2022-704.
   Available:https://doi.org/10.5194/ems2022-704
4. Hoilijoki S, Lipsanen V, Osmane A, Kalliokoski M, George H, Turc L, Kilpua E. Impact of the solar activity on the non-linearity of the statistical dependency between solar wind and the inner magnetosphere. EGU General Assembly 2023, Vienna, Austria. 24–28 April 2023; EGU23-8906.
   Available:https://doi.org/10.5194/egusphere-egu23-8906
5. Carbone F, Telloni D, Yordanova E, Sorriso-Valvo L. Modulation of solar wind impact on the Earth's magnetosphere during the solar cycle. Universe. 2022;8(6): 330.
   Available:https://doi.org/10.3390/universe8060330
6. Shiokawa K. Introduction of Space Weather Research on Magnetosphere and Ionosphere of the Earth. In: Kusano, K. (eds) Solar-Terrestrial Environmental Prediction. Springer, Singapore; 2023.

Available:https://doi.org/10.1007/978-981-19-7765-7_4

7. Syed Zafar SNA, Hazmin SN, Jusoh MH, Dagang AN, Adzni MAM, Umar R. Behaviour of geomagnetic storm, horizontal geomagnetic field and solar wind parameters during solar flare and CMEs event. Journal of Physics: Conference Series, 1768, 2nd International Conference on Space Weather and Satellite Application (ICeSSAT) 2020, Selangor, Malaysia. Published under license by IOP Publishing Ltd; 2020.
   Available:https://doi.org/10.1088/1742-6596/1768/1/012074
8. Pandit D, Chapagain NP, Adhikari B, Mishra RK. Solar activities and its impact on space weather. Proceedings of the International Astronomical Union. 2018; 13(S340):149–150.
   Available:https://doi.org/10.1017/S1743921318001606
9. Riggi F. Detecting Forbush decreases with Geiger counters. In Educational and Amateur Geiger Counter Experiments. UNITEXT for Physics. Springer, Cham. 2024;1-10.
   Available:https://doi.org/10.1007/978-3-031-56960-9_41
10. Dumbović M, Kramarić L, Benko I, Heber B, Vršnak B. A new method of measuring Forbush decreases. Astronomy & Astrophysics. 2024;683:A168.
    Available:https://doi.org/10.1051/0004-6361/202346969
11. Belov AV. Forbush effects and their connection with solar, interplanetary and geomagnetic phenomena. In N. Gopalswamy & D. F. Webb (Eds.), Universal Heliophysical Processes: Proceedings IAU Symposium No. 257, 2008. International Astronomical Union. 2008;439-450.
    Available:https://doi.org/10.1017/S1743921309029676
12. Cane HV. Coronal mass ejections and Forbush decreases. Space Science Reviews. 2000;93(1-2):55–77.
    Available:https://doi.org/10.1023/A:1026532125747
13. Forbush SE. On the effects in cosmic-ray intensity observed during the recent magnetic storm. Physical Review. 1937; 51(12):1108–1109.
    Available:https://doi.org/10.1103/PhysRev.51.1108.3
14. Forbush SE. On world-wide changes in cosmic-ray intensity. Physical Review. 1938;54(12):975–988.
    Available:https://doi.org/10.1103/PhysRev.54.975
15. Davies E, Scolini C, Winslow R, Jordan A. The effect of magnetic reconnection on ICME-related GCR modulation. EGU General Assembly; 2023.
    Available:https://doi.org/10.5194/egusphere-egu23-15621
16. Papailiou M-C, Abunina M, Mavromichalaki H, Shlyk N, Belov S, Abunin A, et al. Precursory signs of large Forbush decreases in relation to cosmic rays equatorial anisotropy variation. Atmosphere. 2024;15(7):742.
    Available:https://doi.org/10.3390/atmos15070742
17. Barrantes M, Valdés-Galicia JF, Musalem O, Hurtado A, Anzorena M, García R, et al. Atmospheric corrections of the cosmic ray fluxes detected by the Solar Neutron Telescope at the summit of the Sierra Negra Volcano in Mexico. Geofísica Internacional. 2018;57(4):253-275.
18. Kilifarska NA, Bakhmutov VG, Melnyk GV. Galactic cosmic rays and solar particles in Earth's atmosphere. In N. A. Kilifarska, V. G. Bakhmutov, G. V. Melnyk (Eds.), The Hidden Link between Earth's Magnetic Field and Climate. Elsevier. 2020;101-131.
    Available:https://doi.org/10.1016/B978-0-12-819346-4.00005-X
19. Melkumyan AA, Belov A, Abunina M, Abunin A, Eroshenko E, Oleneva V, Yanke V. Recurrent and sporadic Forbush decreases during solar cycles 23–24. Solnechno-Zemnaya Fizika. 2019;5(1):39-47.
    Available:https://doi.org/10.12737/szf-51201904 ·
20. Singh YP, Badruddin B. Study of short-term periodicities in the occurrence of Forbush decreases: Wavelet analysis. PREPRINT (Version 1) available at Research Square; 2024.
    Available:https://doi.org/10.21203/rs.3.rs-3901995/v1
21. Melkumyan AA, Belov AV, Shlyk NS, Abunina MA, Abunin AA, Oleneva VA, Yanke VG. Forbush decreases and

geomagnetic disturbances: 1. Events associated with different types of solar and interplanetary sources. Geomagnetism and Aeronomy. 2023;63(6):686–700.
Available:https://doi.org/10.1134/S0016793223600650

22. Melkumyan AA, Belov AV, Abunina MA, Abunin AA, Eroshenko EA, Oleneva VA, Yanke VG. Main properties of Forbush effects related to high-speed streams from coronal holes. Geomagnetism and Aeronomy. 2018; 58(2):154–168.
Available:https://doi.org/10.1134/S0016793218020159

23. Bhaskar A, Subramanian P, Vichare G. Relative contribution of the magnetic field barrier and solar wind speed in ICME-associated Forbush decreases. The Astrophysical Journal. 2016;828(2): 104.
Available:https://doi.org/10.3847/0004-637X/828/2/104

24. Vršnak B, Dumbović M, Heber B, Kirin A. Analytic modeling of recurrent Forbush decreases caused by corotating interaction regions. Astronomy & Astrophysics. 2022; 658:A186.
Available:https://doi.org/10.1051/0004-6361/202140846

25. Kallaya O, Yeeram T. Characteristics of recurrent Forbush decreases in Galactic cosmic ray intensity during positive and negative solar magnetic polarities. Astrophysics and Space Science. 2021;3 66:61.
Available:https://doi.org/10.1007/s10509-021-03970-2

26. Lockwood JA. Forbush decreases in the cosmic radiation. Space Sci Rev. 1971;12: 658–715.
Available:https://doi.org/10.1007/BF00173346

27. Kryakunova O, Belov A, Abunin A, Abunina M, Eroshenko E, Malimbayev A, et al. Recurrent and sporadic Forbush-effects in deep solar minimum. Journal of Physics: Conference Series. 2015;632(1): 012062.
Available:https://doi.org/10.1088/1742-6596/632/1/012062

28. Jämsén T, Usoskin IG, Räihä T, Sarkamo J, Kovaltsov GA. Case study of Forbush decreases: Energy dependence of the recovery. Advances in Space Research. 2007;40(3):342-347.
Available:https://doi.org/10.1016/j.asr.2007.02.025

29. Blanco JJ, Ayuso S, Regadío A, López-Comazzi A, García-Tejedor JI, García-Población Ó, Guerrero Contreras CL. Evolution of the cosmic ray spectrum during a Forbush decrease. Advances in Space Research. 2024;73(9):4842-4852.
Available:https://doi.org/10.1016/j.asr.2024.02.026

30. Munakata K, Kozai M, Kato C, Hayashi Y, Kataoka R, Kadokura A, et al. Large-amplitude bidirectional anisotropy of cosmic-ray intensity observed with worldwide networks of ground-based neutron monitors and muon detectors in 2021 November. The Astrophysical Journal. 2022;938(1):30.
Available:https://doi.org/10.3847/1538-4357/ac91c5

31. Balasis G, Papadimitriou C, Boutsi AZ. Ionospheric response to solar and interplanetary disturbances: A Swarm perspective. Philosophical Transactions of the Royal Society A: Mathematical, Physical and Engineering Sciences. 2019; 377(2154):20180098.
Available:https://doi.org/10.1098/rsta.2018.0098

32. Kataoka R. Disturbed space weather. In R. Kataoka (Ed.), Extreme Space Weather. Elsevier. 2022;31–64.
Available:https://doi.org/10.1016/B978-0-12-822537-0.00005-3

33. Temmer M, Reiss MA, Nikolic L, Hofmeister SJ, Veronig AM. Preconditioning of interplanetary space due to transient CME disturbances. The Astrophysical Journal. 2017;835(2): 141.
Available:https://doi.org/10.3847/1538-4357/835/2/141

34. Richardson IG, Cane HV. Galactic cosmic ray intensity response to interplanetary coronal mass ejections/magnetic clouds in 1995-2009. Solar Physics. 2011;270(2): 609-627.
Available:https://doi.org/10.1007/s11207-011-9774-x

35. Pulkkinen TI. Space weather: Terrestrial perspective. Living Reviews in Solar Physics. 2007;4(1):1-51.

Available:https://doi.org/10.12942/lrsp-2007-1

36. Wimmer-Schweingruber RF. Interplanetary Disturbances Affecting Space Weather. Proceedings of the International Astronomical Union. 2013;8(S300):297–306.
DOI: 10.1017/S1743921313011125

37. Melkumyan AA, Belov AV, Shlyk NS, Abunina MA, Abunin AA, Oleneva VA, Yanke VG. Statistical comparison of time profiles of Forbush decreases associated with coronal mass ejections and streams from coronal holes in solar cycles 23–24. Monthly Notices of the Royal Astronomical Society. 2023;521(3):4544–4560.
Available:https://doi.org/10.1093/mnras/stad772

38. Dumbović M, Vršnak B, Čalogović J, Župan R. Cosmic ray modulation by different types of solar wind disturbances. Astronomy & Astrophysics. 2012;538: A28.
Available:https://doi.org/10.1051/0004-6361/201117710

39. Almasoudi AA, Maghrabi A, Alruhaili A. The impact of several Solar Activity and Geophysical Parameters on the CR muons observed at high cutoff rigidity station. 38th International Cosmic Ray Conference (ICRC2023) - Solar & Heliospheric Physics (SH). 2023;444.
Available:https://doi.org/10.22323/1.444.1322

40. Singh S. Cosmic-Ray Modulation in relation to Solar and Heliospheric Parameters. 38th International Cosmic Ray Conference (ICRC2023) - Solar & Heliospheric Physics (SH). 2023;444.
Available:https://doi.org/10.22323/1.444.1310

41. Rangarajan GK, Barreto LM. Long term variability in solar wind velocity and IMF intensity and the relationship between solar wind parameters & geomagnetic activity. Earth, Planets and Space. 2000; 52(2):121–132.
Available:https://doi.org/10.1186/BF03351620

42. Balan N, Ebihara Y, Skoug R, Shiokawa K, Batista IS, Tulasi Ram S, et al. A scheme for forecasting severe space weather. Journal of Geophysical Research: Space Physics. 2017;122:2824–2835.
Available:https://doi.org/10.1002/2016JA023853

43. Hajra R, Marques de Souza Franco A, Echer E, Bolzan MJA. Long-term variations of the geomagnetic activity: A comparison between the strong and weak solar activity cycles and implications for the space climate. Journal of Geophysical Research: Space Physics. 2021;126:e2020JA028695.
Available:https://doi.org/10.1029/2020JA028695

44. Polatoglu A. Observation of the long-term relationship between cosmic rays and solar activity parameters and analysis of cosmic ray data with machine learning. International Journal of Computational and Experimental Science and Engineering. 2024;10(2).
Available:https://doi.org/10.22399/ijcesen.324

45. Oloketuyi J, Omole O. Investigating the influence of cosmic ray and solar activities on atmospheric weather dynamics within the equatorial electrojet region (Nigeria). Discover Atmosphere. 2024;2:5.
Available:https://doi.org/10.1007/s44292-024-00006-6

46. Hathaway DH. The Solar Cycle. Living Reviews in Solar Physics. 2015; 12:4.
Available:https://doi.org/10.1007/lrsp-2015-4

47. Sawadogo Y, Koala S, Zerbo J. Factors of geomagnetic storms during the solar cycles 23 and 24: A comparative statistical study. Scientific Research and Essays. 2022;17:46–56.
Available:https://doi.org/10.5897/SRE2022.6751

48. Manu V, Balan N, Zhang Q-H, Xing Z-Y. Double superposed epoch analysis of geomagnetic storms and corresponding solar wind and IMF in solar cycles 23 and 24. Space Weather. 2023;21: e2022SW003314.
Available:https://doi.org/10.1029/2022SW003314

49. Garee HS, Hadi KA. Evaluation of the annual correlations between different Solar-Ionospheric indices during solar cycles 23 and 24. Iraqi Journal of Science. 2022;63(10):4587-4600.
Available:https://doi.org/10.24996/ijs.2022.63.10.40

50. Ashruf AM, Bhaskar A, Pant TK. Deciphering solar cycle influence on long-term orbital deterioration of space debris in LEO and MEO orbits. arXiv preprint arXiv:2405.08837; 2024
Available:https://arxiv.org/abs/2405.08837
51. Abe OE, Fakomiti MO, Igboama WN, Akinola OO, Ogunmodimu O, Migoya-Orué YO. Statistical analysis of the occurrence rate of geomagnetic storms during solar cycles 20-24, Advances in Space Research. 2023;71(5) 2240-2251.
52. Belov AV, Eroshenko EA, Oleneva VA, Struminsky AB, Yanke VG. What determines the magnitude of Forbush decreases. Advances in Space Research. 2001;27(3):625–630.
Available:https://doi.org/10.1016/S0273-1177(01)00095-3
53. Belov A, Abunin A, Abunina M, Eroshenko E, Oleneva V, Yanke V, Papaioannou A, Mavromichalaki H. Galactic Cosmic Ray Density Variations in Magnetic Clouds. Solar Physics. 2015;290(5):1429–1444.
Available:https://doi.org/10.1007/s11207-015-0678-z
54. Abunina M, Abunin A, Belov A, Eroshenko E, Oleneva V, Yanke V. Phase distribution of the first harmonic of the cosmic ray anisotropy during the initial phase of Forbush effects. Journal of Physics: Conference Series. 2015;632(1): 012044.
Available:https://doi.org/10.1088/1742-6596/632/1/012044
55. Abunina MA, Abunin AA, Belov AV, Eroshenko EA, Asipenka AS, Oleneva VA, Yanke VG. Relationship between Forbush effect parameters and the heliolongitude of solar sources. Geomagnetism and Aeronomy. 2013;53(1):10–18.
Available:https://doi.org/10.1134/S0016793213010027
56. Papaioannou A, Malandraki O, Belov A, Skoug R, Mavromichalaki H, Eroshenko E, et al. On the Analysis of the Complex Forbush Decreases of January 2005. Solar Physics. 2010;266(1):181–193.
Available:https://doi.org/10.1007/s11207-010-9601-9
57. Chertok IM, Grechnev VV, Belov AV, Abunin AA. Magnetic Flux of EUV arcade and dimming regions as a relevant parameter for early diagnostics of solar Eruptions – Sources of Non-recurrent Geomagnetic Storms and Forbush Decreases. Solar Physics. 2013;282(1): 175–199.
Available:https://doi.org/10.1007/s11207-012-0127-1
58. Veronig AM, Jain S, Podladchikova T, Pötzi W, Clette F. Hemispheric Sunspot Numbers 1874–2020. Astronomy & Astrophysics. 2021;652:A56.
Available:https://doi.org/10.1051/0004-6361/202141195
59. Matzka J, Stolle C, Yamazaki Y, Bronkalla O, Morschhauser A. The geomagnetic Kp-index and derived indices of geomagnetic activity. Space Weather. 2021;19: e2020SW002641.
Available:https://doi.org/10.1029/2020SW002641
60. Borovsky JE, Shprits YY. Is the Dst index sufficient to define all geospace storms? Journal of Geophysical Research: Space Physics. 2017;122:11,543–11,547.
Available:https://doi.org/10.1002/2017JA024679
61. Miteva R, Samwel SW. Catalog of geomagnetic storms with Dst-Index ≤ −50 nT and Their Solar and Interplanetary Origin (1996–2019). Atmosphere. 2023; 14(12):1744.
Available:https://doi.org/10.3390/atmos14121744
62. Zhang X, Song H, Zhang C, Fu H, Li L, Li J, et al. Comparison of ion-proton differential speed between ICMEs and Solar Wind near 1 au. arXiv preprint arXiv:2405.00336; 2024.
Available:https://doi.org/10.48550/arXiv.2405.00336
63. Clette F, Svalgaard L, Vaquero J, Cliver E. Revisiting the sunspot number. Space Science Reviews. 2014;186:35-103.
Available:https://doi.org/10.1007/s11214-014-0074-2.
64. Kamide Y, Kusano K. Is something wrong with the present solar maximum? Space Weather. 2013;11:140–1411.
DOI: https://doi.org/10.1002/ewe.20045
65. Watari S, Kato H, Yamamoto K. Hit rate of space weather forecasts of the Japanese forecast center and analysis of problematic

events on March 2015. Sun Geosph. 2015;10(2): 163–171.
Available:http://newserver.stil.bas.bg/SUNGEO/00SGArhiv/SG_v10_No2_2015-pp-163-171.pdf

66. Okoye, VC, Onuchukwu, CC, Okoli, LN, Okafor-Jerry, OP. Statistical Study of Forbush Effects and Interplanetary Disturbances (FEID) From 1957-2019. Asian Basic and Applied Research Journal V 6(1), 116-131, 2024; .ABAARJ.1653,
Available:https://jofresearch.com/index.php/ABAARJ/article/view/146.

Disclaimer/Publisher's Note: The statements, opinions and data contained in all publications are solely those of the individual author(s) and contributor(s) and not of the publisher and/or the editor(s). This publisher and/or the editor(s) disclaim responsibility for any injury to people or property resulting from any ideas, methods, instructions or products referred to in the content.

© Copyright (2024): Author(s). The licensee is the journal publisher. This is an Open Access article distributed under the terms of the Creative Commons Attribution License (http://creativecommons.org/licenses/by/4.0), which permits unrestricted use, distribution, and reproduction in any medium, provided the original work is properly cited.

Peer-review history:
The peer review history for this paper can be accessed here:
https://prh.globalpresshub.com/review-history/1657